


## Article

# Investigation of the Feasibility of Extracting the Characteristics of Sealed Boxes Using an Automotive FMCW Radar

Lovedeep Singh <sup>1</sup>, Sungjin You <sup>2</sup> , Byung Jang Jeong <sup>2</sup> and Youngwook Kim <sup>3,\*</sup><sup>1</sup> Electrical and Computer Engineering, California State University, Fresno, CA 93740, USA<sup>2</sup> Electronics and Telecommunications Research Institute, Daejeon 34129, Korea<sup>3</sup> Electronic Engineering, Sogang University, Seoul 04107, Korea

\* Correspondence: youngkim@sogang.ac.kr

**Abstract:** This paper investigates the feasibility of extracting the characteristics of sealed paper boxes based on range profiles using a millimeter-wave automotive FMCW radar. Radar is one of the key basic sensors for driving assistance and collision avoidance. Target classification using radar has been studied extensively, yet the detection of sealed material requires further investigation to improve situational awareness for better judgment. We suggest the classification of sealed paper boxes with different materials based on range-profile plots, which capture wave reflection from the box and wave attenuation when traveling through a lossy material. We measure the range profiles of sealed boxes encompassing paper in five different quantities using a millimeter-wave FMCW radar. A theoretical approach is used as a proof of concept, which supports the results of the range-profile measurements. The range profiles of the box with several other materials are also obtained and their characteristics are compared.

**Keywords:** FMCW radar; automotive radar; range profile; permittivity; conductivity; reflection coefficient



**Citation:** Singh, L.; You, S.; Jeong, B.J.; Kim, Y. Investigation of the Feasibility of Extracting the Characteristics of Sealed Boxes Using an Automotive FMCW Radar. *Appl. Sci.* **2022**, *12*, 10243. <https://doi.org/10.3390/app122010243>

Academic Editor: Hosung Choo

Received: 7 September 2022

Accepted: 9 October 2022

Published: 12 October 2022

**Publisher's Note:** MDPI stays neutral with regard to jurisdictional claims in published maps and institutional affiliations.



**Copyright:** © 2022 by the authors. Licensee MDPI, Basel, Switzerland. This article is an open access article distributed under the terms and conditions of the Creative Commons Attribution (CC BY) license (<https://creativecommons.org/licenses/by/4.0/>).

## 1. Introduction

The use of radars in the automotive industry has gained momentum with time, leading to diverse implementations intended to increase safety and offer assistance in driving [1,2]. Vehicles made in the past decade most likely contain some use of radar, including vehicle detection, adaptive cruise control, and range-based collision alerts. Radar is one of the critical sensors for automotives, because it operates regardless of weather and light conditions, unlike optical systems. Furthermore, radar is less expensive than lidar systems.

Radar technology is advancing to improve self-driving vehicles' safety features through accurate target detection and classification. Radar-based object detection and tracking were addressed in [3,4], especially for multiple target detection purposes. In [5], the automotive use of radar systems for classification was discussed. In the paper, vehicles, clutter, roadside objects, and humans were classified through time-varying features in the range-Doppler diagram. Data from radar, as well as lidar, are considered together for better object detection through data fusion algorithms [6]. In addition, an approach that employed both radar and a camera was studied to improve target detection accuracy [7,8]. However, further improvements to classification are needed when self-driving vehicles face unknown and nonvisual objects during a trip, using the material-based classification of sealed objects to decide whether a vehicle should avoid the object for the safety of passengers and other drivers. Knowing the composition of the sealed object can greatly increase safety by allowing the classification of contact with an unknown object as harmful. Generally, a self-driving vehicle will stop under such circumstances, but a sudden stop can endanger other vehicles. Even though the classification of concealed materials is impossible for human drivers or optical systems, electromagnetic waves have the ability to penetrate visually opaque objects such as a cardboard box and provide information pertaining to the materials inside the box.

Previous work has been done on material classification by incorporating comb-based millimeter-wave detectors, which focused on material and thickness classification that correlates with our classification for lighter and denser materials [9]. Similarly, FMCW radars have been used to classify materials including carpet, tile, liquid, and laminate based on range cross-range images [10]. There has also been prior work that concludes material classification based on unique power dissipation because of a material's exclusive dielectric properties [11]. Furthermore, radar systems have already been used in specific environments to classify objects that are not visible. Ground-penetrating radars have been used to detect land mines due to their ability to penetrate through the soil and concealed object classification has been used to detect hazardous material for security purposes [12,13]. Such uses are practical for radar, which can classify materials and substances without relying on visual indications. However, to the best of the authors' knowledge, radar has not been attempted for the classification of sealed objects in automotive applications.

In this paper, we investigate the feasibility of classifying a sealed paper box through range profiles measured using an FMCW radar operating at 77 GHz. We use a range profile to differentiate between different materials by analyzing attenuation over distance as an incident wave propagates through the material. Similarly, this concept of range profile has been used in [14] to determine a pipe wall's thickness. This experiment is conducted using a 56 cm × 40.6 cm × 38.1 cm packaging box filled with five different quantities of paper, corresponding to the five stages. We use crumpled papers because it is convenient to control the paper density of the box. The range profile of each stage is unique in its dissipation of the incident wave. The range profile provides the reflected wave at the front and back ends of the box. The front provides the initial reflected wave, which is then compared with the second peak, the reflected wave at the back of the box. Depending on the material inside the box, attenuation differs. If a light, low-density material is enclosed in the box, the attenuation between the two reflections at the front and back end of the box will be low, whereas a dense or heavy material that has generally high permittivity or high conductivity produces larger attenuation over the same distance. Accordingly, we use a range profile to classify the box with a material that is to be avoided. A theoretical approach is also conducted to further verify the obtained measurement results. Plane-wave propagation/reflection provides a theoretical background for later comparison with measurements made using the FMCW radar. After checking the feasibility of classifying different densities of the papers, we also investigate other materials: bubble wrap, clothes, water bottles, garden soil, mulch, and granite pebbles. The range profiles of these different materials are analyzed to further investigate the feasibility of determining the potentially dangerous materials on the road.

This paper is organized as follows: Section 2 defines the theoretical approach, focusing on deriving the equations for reflections in the front and back ends of the box. Section 3 compares measurements obtained from the radar measurements with calculations made using the theoretical approach. Section 4 focuses on other materials, and Section 5 provides a discussion. Section 6 offers our conclusion.

## 2. Theoretical Approach

To investigate the feasibility of estimating material density inside a cardboard box for the purposes of automobile safety, we use crumpled paper, whose density can easily be controlled by using different numbers of sheets. In addition, we can simulate light materials to heavy materials depending on the quantity of paper. We assume that randomly accumulated papers are uniformly distributed in the box. It is necessary to analyze the radar returns theoretically to later verify measurement results by calculating the magnitude of reflections from the sealed box. When the electromagnetic wave from the radar impinges the box located on the road, it is expected that the major reflections will occur in two boundaries, (i) from air to box and (ii) from box to air, as noted in Figure 1a. These reflections produce two corresponding peaks in the range profile, as demonstrated in Figure 1b. Even though there are multiple peaks from multiple reflections, two peaks are

dominantly observed in the range profile because other echoes from multiple reflections experience severe attenuation due to a long pathway. To calculate the magnitudes of the peaks,  $A_1$  and  $A_2$ , that are related to the material characteristics inside, we used a five-layer model consisting of air, cardboard box, enclosed material, cardboard box, and air. The problem setup is demonstrated in Figure 2.

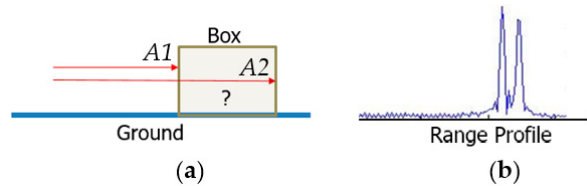


Figure 1. (a) Problem setup, and (b) expected range profile.

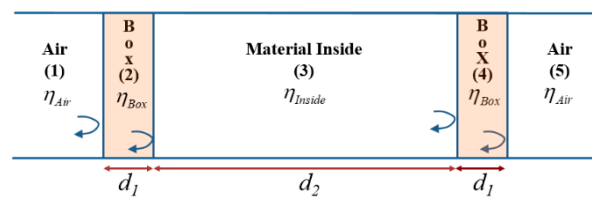


Figure 2. Five-layer model of the cardboard box. Curved arrows represent reflection.

For the theoretic estimation of the magnitudes of  $A_1$  and  $A_2$ , the reflection coefficient and the transmission coefficient should be calculated at each boundary. The reflection coefficients are found using the intrinsic impedance values that are the respective values for permeability and permittivity.

$$\Gamma_{NM} = \frac{\eta_M - \eta_N}{\eta_M + \eta_N}, T_{NM} = 1 - \Gamma_{NM} \tag{1}$$

where  $\eta$  is intrinsic impedance,  $\Gamma_{NM}$  is the reflection coefficient between the  $M$ th and  $N$ th layers, and  $T_{NM}$  is the transmission coefficient between the  $M$ th and  $N$ th layers. The electromagnetic characteristics of the material, the permittivity, and the permeability of five layers are required to calculate wave impedance, the propagation constant, and the attenuation constant. Because the materials considered are nonmagnetic, the relative permeability is set to 1 for all layers. The relative permittivity of the cardboard box was found to be 1.78 [15]. The dielectric constant of paper can range from 1.7 to 4.0 depending on the manufacturing characteristics, humidity, and paper composition [16]. In this study, the permittivity values were unique in each case because of the different densities of paper at each stage. The dielectric constant for the last stage, the densest, was found by calculating a value that provided high attenuation, resulting in a negligible magnitude for the second reflection. The last stage, which had the most paper, dissipated the most energy from the incident wave. The  $\epsilon$  values for the first four stages were calculated under the assumption that they are linearly proportional to the paper quantity per stage, referring to stage five. Besides, the cardboard and paper exhibited conductivity, producing complex permittivity.

$$\epsilon_c = \epsilon' - j\epsilon'' = \epsilon' - j\frac{\sigma}{\omega} \tag{2}$$

The complex component  $\epsilon''$  can be found using the operating frequency of the radar and the electric conductivity of the material. The cardboard and printer paper are both made of wood, whose conductivity varies from  $10^{-4}$  to  $10^{-3}$  (S/m) depending on humidity and the manufacturing of the material [17]. The electric conductivity value of  $10^{-3}$  was used for the cardboard box. The conductivity value of  $\sigma = 0.000468$  (S/m) was chosen for the last stage. For other stages, it was assumed that the number of papers inside the box per stage was linearly proportional to conductivity. Table 1 shows paper quantity, dielectric constant, and conductivity values per stage used in the simulation.

**Table 1.** Quantity, permittivity, and conductivity per stage.

Stage	Paper Quantity	Relative Permittivity	Conductivity (S/m)
1	44	1.09	0.000063
2	75	1.15	0.000107
3	126	1.25	0.000180
4	197	1.39	0.000282
5	327	1.65	0.000468

Materials with  $\sigma > 0$  will dissipate energy when the wave propagates. Each of the five stages contains a different amount of paper or quantity of lossy material inside the box, for a unique amount of energy dissipation at each stage. For low-lossy material, the propagation constant,  $\beta$ , and the attenuation constant,  $\alpha$ , are found using the Binomial expansion:

$$\alpha = \frac{\omega \epsilon''}{2} \sqrt{\frac{\mu}{\epsilon'}} = \frac{\sigma}{2} \sqrt{\frac{\mu}{\epsilon'}}, \beta = \omega \sqrt{\mu \epsilon'} \cdot \left( 1 + \frac{1}{8} \left( \frac{\epsilon''}{\epsilon'} \right)^2 \right) \tag{3}$$

As we have all the material parameters, we can calculate the magnitude of two peaks. The magnitude of the first peak,  $A_1$ , is calculated by summing the two echoes. The first echo is from the boundary between air (1) and the cardboard box (2), and the second echo is from the boundary between the cardboard box (2) and the material inside (3). These two echoes overlap in the range profile because the thickness of the cardboard box (1 cm) is less than the range resolution (5.02 cm) of the radar. It should be noted that the phase delay and attenuation factor are considered in the equation:

$$A_1 = M \cdot \Gamma_{12} + M \cdot T_{12} \cdot \Gamma_{23} \cdot T_{21} \cdot e^{-j\beta_{\text{box}} \cdot 2d_1} \cdot e^{-\alpha_{\text{box}} \cdot 2d_1} \tag{4}$$

where  $M$  is the magnitude of the incident wave,  $d_1$  is the thickness of the box, and  $d_2$  is the length of the box inside. The magnitude,  $A_2$ , of the second peak in the range profile comes from the third boundary between the material inside (3) and the cardboard box (4), as well as the fourth boundary between the cardboard box (4) and air (5). Again, because the thickness of the cardboard is less than the range resolution of the radar, we observe only one peak from the two reflections.  $A_2$  can be calculated as:

$$A_2 = M \cdot T_{12} \cdot T_{23} \cdot \Gamma_{34} \cdot T_{32} \cdot T_{21} \cdot e^{-j\beta_{\text{box}} 2d_1} \cdot e^{-\alpha_{\text{box}} 2d_1} \cdot e^{-j\beta_m 2d_2} \cdot e^{-\alpha_m 2d_2} + M \cdot T_{12} \cdot T_{23} \cdot T_{34} \cdot \Gamma_{45} \cdot T_{43} \cdot T_{32} \cdot T_{21} \cdot e^{-j\beta_{\text{box}} 4d_1} \cdot e^{-\alpha_{\text{box}} 4d_1} \cdot e^{-j\beta_m 2d_2} \cdot e^{-\alpha_m 2d_2} \tag{5}$$

where the subscript of  $m$  means the material inside. It is expected that the difference between  $A_1$  and  $A_2$  comes mainly from the attenuation in the material, as the reflection coefficient between air and box is small.

Based on the material properties at each stage and the physical size of the cardboard box, the magnitudes of the two peaks are calculated. The results for attenuation per stage, the ratio between the second peak and the first peak, were obtained, as shown in Table 2. It is observed that the higher conductance results in a higher attenuation constant. These ratios of attenuation are compared with the measurement results in the next section.

**Table 2.** Attenuation for all five stages using simulation and measurement.

Stage	Simulated Attenuation	Measured Attenuation
I	0.89281	0.89205
II	0.57376	0.46242
III	0.25906	0.29256
IV	0.07659	0.06288
V	0.00661	0.03114

### 3. Measurements and Results

To obtain the measured range profile, a millimeter-wave FMCW radar made by TI Co., Ltd. was used. An FMCW radar is an ideal choice for short and medium-range applications, being low-cost and easy to use. The AWR1243 radar we used operates at 77 GHz. For our case, the most important factor was range resolution, which is affected by the bandwidth swept by the chirp and the sampling rate. A better range resolution can differentiate between two targets at a smaller distance but also shortens the range in view for the radar because of the limited sampling rate. A range resolution of 5.02 cm and a range of 6.4 m were obtained using the following parameters: operating frequency of 77 GHz, bandwidth swept by 2987 MHz, A/D sampling rate of 3 MHz, chirp rate of 70.006 MHz/ $\mu$ s, 128 chirps per frame, and 24 frames per burst.

The five different stages of enclosed printer paper quantity are shown in Table 1. For each stage, the target box was placed at the same spot to avoid any discrepancies from changing the target location and orientation. The target box's front end was 3 m from the radar for each stage. The distance between the two ends of the box, 56 cm, was confirmed by the distance between the two peaks in the range profile. Each stage of the box was entirely filled with crumpled paper. The increasing density of paper per stage was achieved by crumpling the papers into smaller wads. Figure 3 shows the placement of the box in front of the radar, and Figure 4 shows a top view of the five different stages of paper density.

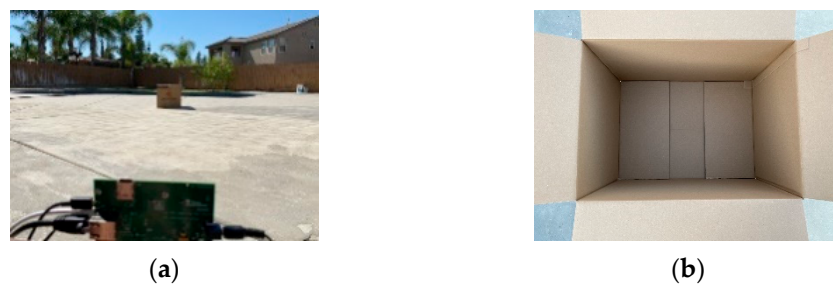


**Figure 3.** (a) The measurement setting with radar and (b) an empty box.

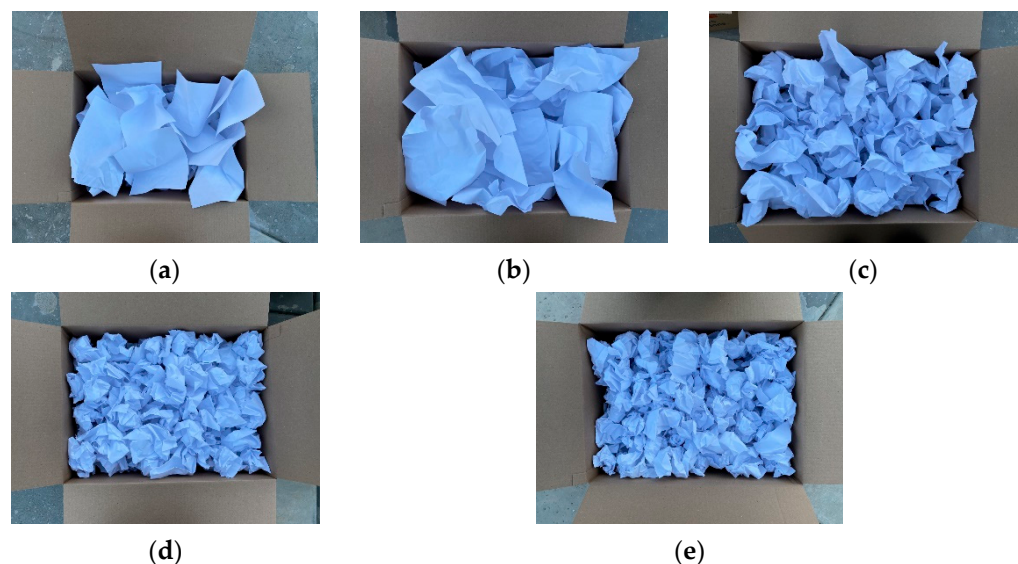


**Figure 4.** Visual of the five different stages of paper quantity; (a) Stage I, (b) Stage II, (c) Stage III, (d) Stage IV, and (e) Stage V.

After the target box was placed, the mmWave Studio provided by TI Co. Ltd (Dallas, TX, USA). was used to input the discussed parameters to obtain the radar data. As all data were captured for every stage, the data were then processed in MATLAB to obtain each range profile. Zero-padding was used in the FFT process to obtain a detailed range profile.



The resulting plot formulates the two peaks of reflection magnitudes required to obtain an attenuation ratio, which is obtained by comparing the magnitudes of the two peaks. The magnitude of the first peak is roughly in the same range for all stages, but we are only focusing on the attenuation for the two peaks because the second peak will be affected by the paper density of the box. Figure 5 presents the results obtained for the empty box as well as the five stages.

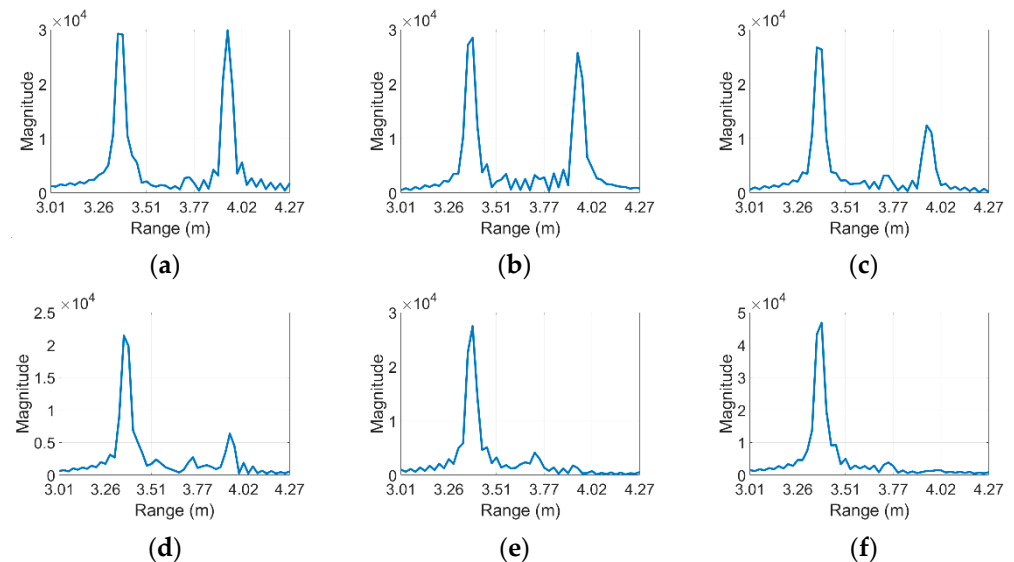


**Figure 5.** Range-profiles for (a) an empty box, (b) stage 1, (c) stage 2, (d) stage 3, (e) stage 4, and (f) stage 5.

The empty stage, presented in Figure 5a, shows both reflection magnitudes roughly equal to each other because the attenuation of the electromagnetic wave inside the box is negligible. The only effect of power dissipation occurs from the two thin layers of the cardboard box, which introduce complex permittivity. Each of the following five stages shows power dissipation with increased paper quantity. Stage V was packed with the highest amount of paper for almost 100% power dissipation, with the second peak absent. Table 2 shows the attenuation ratio between the two peaks for every stage. It is noted that adding permittivity in between shifts the second peak due to the different propagation time delay. However, the amount is so small that we could not observe it in our experiments.

The results obtained for measurements and calculations were close for most stages. Differences in attenuation might result from the general makeup of the material, including factors relating to humidity and the specific species of wood used, which produce unique degrees of permittivity and conductivity. However, both datasets agree in demonstrating the concept of material classification based on power dissipation as a result of the material makeup, with similar trends in attenuation.

#### 4. Other Materials

We also measured the range profile of other materials: bubble wrap, clothes, water bottles, gardening mulch, and granite pebbles. These materials were chosen to simulate an experiment in which materials of varying densities are analyzed. Each material filled the whole volume of the same box. The least dense material was bubble wrap, which has air pockets inside, whereas granite pebbles were the heaviest and densest. Boxes of different materials are shown in Figure 6, and their corresponding range profiles are presented in Figure 7.

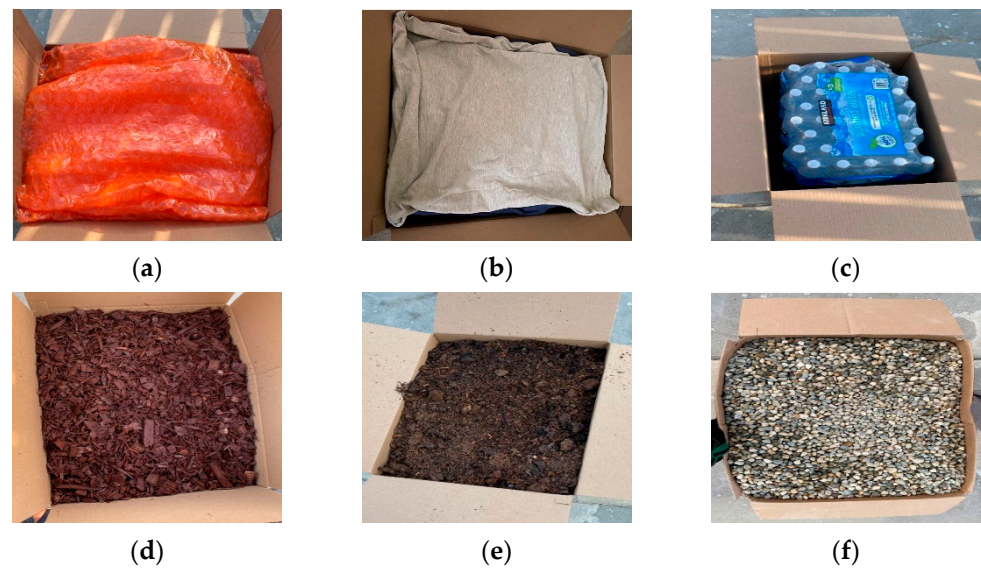


**Figure 6.** Materials used for range-profile capture: (a) bubble-wrap; (b) clothes; (c) water; (d) mulch; (e) soil; and (f) granite pebbles.

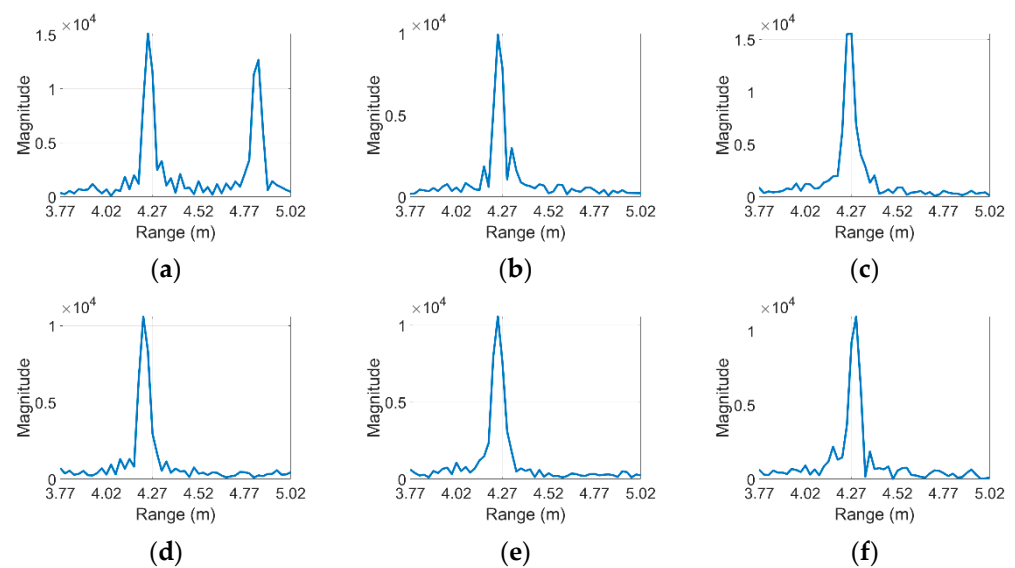


**Figure 7.** The range-profile plot of the following materials: (a) bubble-wrap; (b) clothes; (c) water; (d) mulch; (e) soil; and (f) granite pebbles.

Based on the range-profile plots shown in the figure, only bubble wrap had a second reflection from the back of the box. This material will cause a lesser impact on the automobile when hit owing to its relatively low mass. Other materials with high relative permittivity and conductivity can severely damage automobiles due to their high mass. In these cases, we observed no significant reflection from the back end of the box because the reflection from the front as well as the attenuation constant was high. Based on the ratio between the first peak and the second peak, we can observe the potential feasibility of identifying a sealed box that is potentially dangerous.

## 5. Discussion

There are a few limitations to be addressed when the suggested method is applied in realistic scenarios. For the measurements made during the five stages shown in Table 2, we placed the box perpendicular to the radar's boresight. However, it is also important to study measurement results when a box is placed at several different angles. We found that

orientation changes of more than about 15 degrees lowered the magnitudes close to the noise levels in measurements as the RCS became small. Accordingly, the proposed concept is valid when the incident angle of the radar wave is near 90 degrees.

The use of this technique will be limited if the box is partially filled with materials. In principle, there will be two returns that arrive at the Rx of the radar; one that passes through the air and the other that passes through the material. If the time delay difference between the air and the material is not significant, the two returns will be co-located in the range profile, which makes it hard to discern them. In the range profile, the return that passes air will be dominant, as its amplitude is higher.

In addition, there are cases where the reflection from the box is not strongly related to the mass of the material, for example, an empty box covered by aluminum foil. While aluminum foils will produce a strong return, the mass is small. The suggested method may cause an erroneous decision as to whether or not to collide with an object.

It is also noted that scattering and penetration characteristics are a function of the carrier frequency. With the increase in frequency, the amount of penetration decreases while reflection/scattering becomes more significant. Therefore, the lower frequency is preferable in this scenario as the suggested approach uses the penetration characteristic.

## 6. Conclusions

This study investigated the feasibility of classifying potentially dangerous materials sealed inside a box based on range-profile data obtained using a millimeter-wave FMCW radar. By varying quantities of paper, we measured the five stages of a sealed cardboard box and found that the paper density is highly related to the power dissipation through propagation inside the box. Attenuation was identified by the magnitude difference between two peaks in the range profile. The theoretical approach also supported the effect of these factors by simulating each stage and comparing it with the measurement results. When the box was filled with light or low-density materials, a small attenuation at a second peak was observed.

However, many limitations need to be overcome to advance this study for the purposes of material classification. The RCS of the target object is a major factor in obtaining reliable data that can be processed for classification, especially when the distance to the radar is far. The values used for the relative permittivity and conductivity of paper can vary greatly with manufacturing characteristics and humidity. The specific paper and cardboard material's properties should be obtained more accurately, which should provide a better output from simulated calculations.

**Author Contributions:** Conceptualization, Y.K., S.Y., and B.J.J.; methodology, L.S. and Y.K.; software, L.S.; validation, L.S. and Y.K.; formal analysis, L.S.; investigation, L.S.; data curation, L.S.; writing—original draft preparation, L.S. and Y.K.; writing—review and editing, S.Y. and B.J.J.; visualization, L.S.; supervision, S.Y. and B.J.J.; project administration, S.Y. and B.J.J.; funding acquisition, S.Y. and B.J.J. All authors have read and agreed to the published version of the manuscript.

**Funding:** This research was supported in part by Electronics and Telecommunications Research Institution (ETRI) grant funded by the Korean government (22ZH1100, Study on 3D Communication Technology for Hyperconnectivity).

**Institutional Review Board Statement:** Not applicable.

**Informed Consent Statement:** Not applicable.

**Data Availability Statement:** Not applicable.

**Conflicts of Interest:** The authors declare no conflict of interest.



## References

1. Hasch, J.; Topak, E.; Schnabel, R.; Zwick, T.; Weigel, R.; Waldschmidt, C. Millimeter-wave technology for automotive radar sensors in the 77 GHz frequency band. *IEEE Trans. Microw. Theory Tech.* **2021**, *60*, 845–860. [[CrossRef](#)]
2. Smith, K.; Csech, C.; Murdoch, D.; Shaker, G. Gesture recognition using mm-wave sensor for human-car interface. *IEEE Sens. Lett.* **2018**, *2*, 3500904. [[CrossRef](#)]
3. Manjunath, A.; Liu, Y.; Henriques, B.; Engstle, A. Radar based object detection and tracking for autonomous driving. In Proceedings of the IEEE MTT-S International Conference on Microwaves for Intelligent Mobility, Munich, Germany, 15–17 April 2018.
4. Hussain, M.; Azam, S.; Munir, F.; Khan, Z.; Jeon, M. Multiple objects tracking using radar for autonomous driving. In Proceedings of the IEEE International IOT, Electronics and Mechatronics Conference, Vancouver, BC, Canada, 9–12 September 2020.
5. Kim, Y.; Alnujaim, I.; You, S.; Jeong, B. Human detection based on time-varying signature on range-Doppler diagram using deep neural networks. *IEEE Geosci. Remote Sens. Lett.* **2020**, *18*, 426–430. [[CrossRef](#)]
6. Aldrich, R.; Wickramaratna, T. Low-cost radar for object tracking in autonomous driving: A data-fusion approach. In Proceedings of the IEEE 87th Vehicular Technology Conference, Porto, Portugal, 3–6 June 2018.
7. Abdalwohab, M.; Zhang, W.; Abdelgader, A.; Abdelazeem, I. Deep learning based camera and radar fusion for object detection and classification. In Proceedings of the IEEE 4th International Conference on Automation, Electronics and Electrical Engineering, Shenyang, China, 19–21 November 2021.
8. Nabati, R.; Qi, H. CenterFusion: Center-based radar and camera fusion for 3D object detection. In Proceedings of the IEEE Winter Conference on Applications of Computer Vision, Waikoloa, HI, USA, 3–8 January 2021.
9. Jamali, B.; Ramalingam, D.; Babakhani, A. Intelligent material classification and identification using a broadband millimeter-wave frequency comb receiver. *IEEE Sens. Lett.* **2020**, *4*, 3501104. [[CrossRef](#)]
10. Weib, J.; Santra, A. One-shot learning for robust material classification using millimeter-wave radar system. *IEEE Sens. Lett.* **2018**, *2*, 7001504.
11. Shylo, S.; Harmer, S. Millimeter-wave imaging for recycled paper classification. *IEEE Sens. J.* **2016**, *16*, 2361–2366. [[CrossRef](#)]
12. Yoldemir, B.; Sezgin, M. A least squares approach to buried object detection using ground penetrating radar. *IEEE Sens. J.* **2011**, *6*, 1337–1341. [[CrossRef](#)]
13. Andrews, D.; Harmer, S.; Bowring, N.; Rezgui, N.; Southgate, M. Active millimeter wave sensor for standoff concealed threat detection. *IEEE Sens. J.* **2013**, *13*, 4948–4954. [[CrossRef](#)]
14. Jebramcik, J.; Rolfes, I.; Pohl, N.; Barowski, J. Millimeterwave radar systems for in-line thickness monitoring in pipe extrusion production Lines. *IEEE Sens. Lett.* **2020**, *4*, 6000504. [[CrossRef](#)]
15. Khonsari, Z.; Björninen, T.; Tentzeris, M.; Sydänheimo, L.; Ukkonen, L. 2.4 GHz inkjet-printed RF energy harvester on bulk cardboard substrate. In Proceedings of the IEEE Radio and Wireless Symposium (RWS), San Diego, CA, USA, 25–28 January 2015; pp. 153–155.
16. Markell, J.; Baker, E.; Gu, G.; Joseph, I.; Lansdowne, C.; Thakkar, R.; Zhou, E.; Zhou, R.; Ye, J. *Calculating the Relative Permittivity Constants of Various Dielectric Materials Using a Parallel Plate Capacitor*; Science Department, All Saints Episcopal School: Tyler, TX, USA, July 2016.
17. James, W. *Electric Moisture Meters for Wood*; General Technical Report; U.S. Department of Agriculture: Washington, DC, USA, 1988; pp. 1–16.